THE JOURNAL OF PHYSICAL CHEMISTRY A

 VOLUME 106, NUMBER 24, JUNE 20, 2002

FEATURE ARTICLE

Mapping Reaction Dynamics via State-to-State Measurements: Rotations Tell the Tale

James J. Valentini*

Department of Chemistry, Columbia University, New York, New York 10027

Received: January 14, 2002; In Final Form: March 13, 2002

We describe a series of experiments and computational simulations of the state-to-state dynamics of the atom transfer reactions H + HX → $H_2(v',j')$ + X (HX = hydrogen halide) and H + RH → $H_2(v',j')$ + R (RH = alkane). The rotational and vibrational state distributions of the H_2 products are characterized for reaction at well-defined initial conditions. The vibrational state distributions provide some information. However, it is the rotational state distributions that form the basis for mapping the path from reactants to products. In analyzing these state distributions, we develop a method that takes explicit, quantitative account of kinematic constraints on the product energy disposal. This method is generally applicable to bimolecular reactions and provides a context in which to interpret the rotational and vibrational state distributions.

I. Introduction

When we have elaborated a reaction scheme in terms of a series of elementary reaction steps, we have achieved a certain understanding of the chemical transformation of reactants into products. The elementary reaction steps represent the individual chemical events that lead to the overall reaction. When we can study the individual reaction steps separately and characterize them by Arrhenius parameters, we have reached the end of one inquiry of the reaction process. For example, for the reaction that overall is given by $H_2 + Br_2 \rightarrow 2HBr$, it is known by every student who has taken a kinetics course that the reaction proceeds by the simple series of elementary steps:[1]

$Br_2 + M \rightarrow 2Br + M$	initiation
$Br + H_2 \rightarrow HBr + H$	propagation
$H + Br_2 \rightarrow HBr + Br$	propagation
$H + HBr \rightarrow H_2 + Br$	inhibition
$2Br + M \rightarrow Br_2 + M$	termination

Each of these steps can be and has been studied experimentally to determine Arrhenius parameters, and by them the kinetics of the overall reaction is determined.

From a different perspective, that of chemical reaction dynamics, understanding has not yet been achieved.[2] The question of how, in terms of the motion of the individual atoms, each elementary reaction breaks old bonds and makes new ones is unanswered and in fact is yet to be posed. Though each elementary reaction represents the species that collide and react, why this occurs in the way it does is not revealed. From this perspective, the interesting information is hidden within the arrow that separates the reactants from products and indicates the direction of the reaction. That arrow has the same import as the one we would write to indicate the origin and destination of a trip, as in New York → Los Angeles; namely, it contains the path that has been taken.

To describe the path of a trip we use a map, and similarly, to describe the path of a reaction, we want to produce a map. The differences between the two though are great. The path in our travels is in a space of two mathematical dimensions, latitude and longitude say, or three dimensions if we also include altitude. That of our reactions is in a $3n - 6$ dimensional hyperspace. The path in our travels can be derived from and represented in a map that exists independently of the trip and is available to us at all times, and the trip can be followed easily in real time. The map for our reaction exists only during the

* To whom correspondence should be addressed. Mailing Address: Department of Chemistry, Columbia University, 3000 Broadway, MC 3120, New York, NY 10027. E-mail: jjv1@chem.columbia.edu. Phone: 212-854-7590. Fax: 212-932-1289.

10.1021/jp0201027 CCC: $22.00
Published on Web 05/11/2002

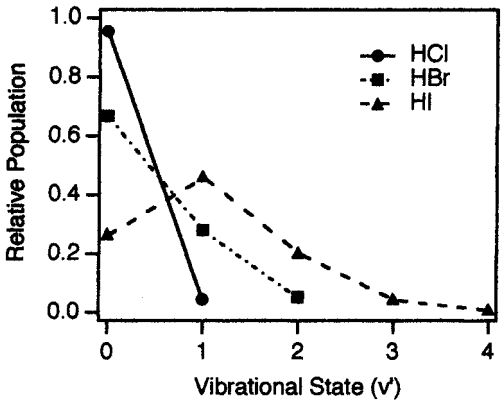

Figure 1. Vibrational state distributions for the H_2 product of the reactions of H with HCl, HBr, and HI at 1.6 eV collision energy. Error bars on the experimental data have been removed to make comparison of data clearer. Differences among the reactions are much larger than the error bars associated with any of the data.

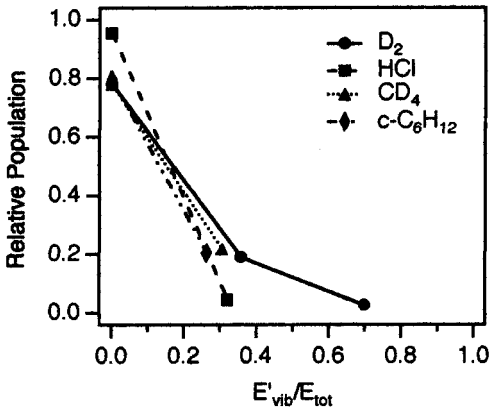

Figure 2. Vibrational state distributions for the H_2 or HD product of the reaction of H with D_2, HCl, CD_4, and *c*-C_6H_{12}, plotted as a function of reduced vibrational energy at a collision energy of 1.3 eV for H + D_2 and 1.5−1.6 eV for the others. Error bars on the experimental data have been removed to make comparison of data clearer. Here the error bars are comparable to the differences among the different reactions.

reaction, and it presents itself on a time scale as short as a few femtoseconds.

State-to-state dynamics nonetheless aims to produce such a map of the connections between the reactants and products.[2] However, it does so in an indirect way. In effect, we treat the reaction process as a black box, which has locked inside it the map that establishes the connections between reactants and products. We try to discern the features of the map by observing how specific quantum states of the reactants lead to particular quantum states of the products. We cannot expect that all the aspects of the map may be revealed by these measurements, but the measurements can be so numerous as to tightly constrain any model of the reaction, which in another way expresses this map. Generally, computational simulation of the reaction can lead to more detail and more accuracy and more insight in our characterization of the reaction than can experiment alone. So in this, the results of the state-to-state dynamics experiments function effectively to test the simulations so that they can be more confidently accepted.

For reactions on a single adiabatic potential energy surface, the quantum states of the reactants and products that we need to prepare and measure are those of the vibrations and rotations of the reactants and products. The connections between a particular vibrational state of the reactants and another for the products is obviously a sensitive probe of the reaction map. This state-to-state connection expresses the coupling between a particular set of bonds in the reactants and a different set of bonds involving the same atoms in the products. An examination of the available data shows that the vibration-to-vibration state-to-state dynamics is sensitive to two aspects of the map of the reaction dynamics. These are the exoergicity, which determines where along the reaction coordinate the saddle point lies, and whether a particular bond persists throughout the reaction or is broken/formed.

Figure 1 shows the $v = 0 \rightarrow v'$ vibrational state-to-state probabilities for the H + HX → H_2 + X (HX = HCl, HBr, HI) reactions.[3] (Our notation here uses unprimed v and j to indicate reactant vibrational and rotational quantum numbers and the primed variables v' and j' to denote the same for the products. Though spectroscopy is used to measure the distribution of products over vibrational and rotational states, the notation used here is not that of spectroscopy but rather that of dynamics.) These three reactions have very characteristic state-to-state vibrational probabilities. This is due to their very different thermochemistry, $\Delta H_0 = -0.05$, -0.72, and -1.42 eV,[4] respectively, and the consequent variation of the location of the saddle point for each. At the saddle point, the r_{HH} distance is 0.95, 1.13, and 1.99 Å for HCl,[5] HBr,[6] and HI,[6] respectively, compared to an equilibrium r_{HH} in H_2 of 0.742 Å.[7]

Experiments with vibrationally excited H_2O in the H + H_2O → H_2 + OH reaction illustrate how the product vibrational state distribution reveals the differentiation between persistent and reacting bonds. Reaction studies have been done on this system using vibrational overtone pumping to prepare highly excited local modes of H_2O.[8,9] In these experiments, the collision energies are those of a room temperature thermal sample, and the substantial reaction barrier (0.93 eV)[10−13] can be surmounted only if an OH bond in the H_2O reactant is highly excited vibrationally. From a reactant state having one quantum in one OH stretch and three quanta in the other, the OH product is formed predominantly in $v' = 1$. For excitation of the H_2O to a vibrational level with four quanta in one of the local OH modes and none in the other, the OH is formed predominantly in $v' = 0$. So, reaction occurs at the vibrationally excited OH bond in H_2O, whereas the other OH bond in H_2O acts as a spectator and its vibrational energy adiabatically evolves into OH product vibration.

When several reactions have similar thermochemistry, the vibrational distributions are very similar, as Figure 2 shows. Here, we have plotted the vibrational state distribution for the reaction of an H atom with ground vibrational state D_2, [14,15] HCl,[3] CD_4,[16] and *c*-C_6H_{12},[17] at a collision energy of 1.3 eV for H + D_2 and 1.6 eV for the others. The plot is probability versus reduced vibrational energy rather than vibrational quantum number to account for the difference in the vibrational energy levels of HD and H_2.

In all four reactions, the product vibrational state distribution peaks strongly at $v' = 0$ with only very small amount of $v' = 1$, and in the case of H + D_2 a bit of $v' = 2$. No error bars are shown for these experimental measurements to make it easier to see the multiple plots. That absence makes it important to note that the four vibrational distributions are essentially identical within their mutual uncertainties.

The first three of these reactions are very close to thermoneutral, with $\Delta H_0 = 0.04$, -0.05, and 0.09 eV.[4] The fourth, H + *c*-C_6H_{12} is mildy exoergic, with $\Delta H = -0.38$ eV.[4] However, this is not enough to make its vibrational state distribution very different from the others. That thermochemistry places the H + *c*-C_6H_{12} reaction energetically just about exactly halfway

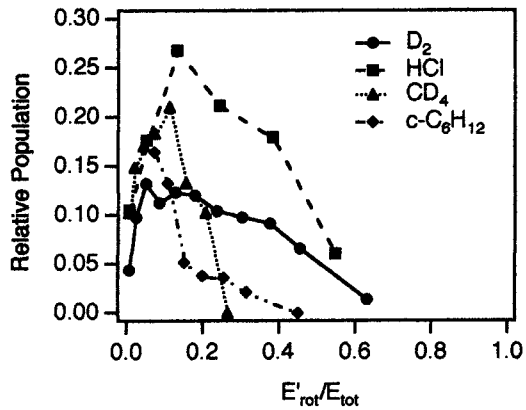

Figure 3. Rotational state distributions for the H_2 or HD $v' = 0$ product of the reactions of H with D_2, HCl, CD_4, and c-C_6H_{12}, plotted as a function of reduced rotational energy. Collision enegies are the same as those in Figure 2. Error bars on the experimental data have been removed to make comparison of data clearer. Differences among the reactions are larger than the error bars associated with any of the data.

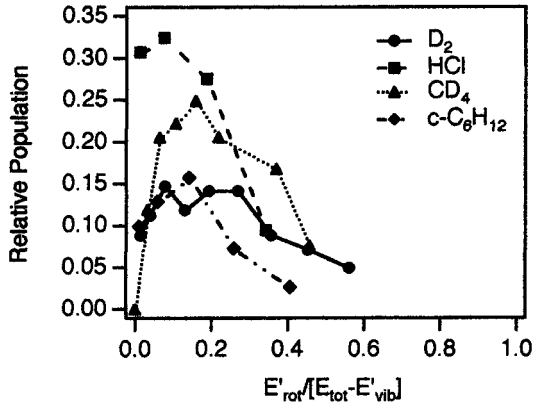

Figure 4. As in Figure 3, except for products in $v' = 1$.

between H + HCl and H + HBr. Figure 1 shows that this should make the H + c-C_6H_{12} reaction much like the nearly thermoneutral reactions with which we compare it in Figure 2.

Figure 2 shows something else as well, that the vibrational state distributions are quite cold even when the collision energy is very high. At the 1.3 eV/1.6 eV collision energies at which these vibrational state distributions were determined, there is enough energy to populate states up to $v' = 3$ for H + D_2 and $v' = 4$ for H + c-C_6H_{12}. However, reactant translation does not evolve into product vibration to any real extent. The average energy disposal into product vibration is a small fraction of the collision energy. We will reconsider this later in this review. Its explanation is the source of a different way to make energy plots such as that of Figure 2 and a better way to analyze the energy disposal into all degrees of freedom.

Figures 3 and 4 compare the $v' = 0$ and $v' = 1$ rotational state distributions for these four reactions, again plotted on a reduced energy scale to account for the different rotational constants of H_2 and HD. These are decidedly different. This is a specific example of what we have generally found: the rotational state distributions are quite characteristic and differentiating.

This seems intuitively reasonable, for several reasons. The rotational state distributions are constrained by both energy conservation and angular momentum conservation. Under the conditions of many state-to-state dynamics experiments, the total angular momentum is determined almost entirely by the reactant orbital angular momentum, and so the angular momentum directly reflects the opacity function. Rotational energy release is conditioned by the geometry at the transition state, so the distributions reflect that geometry as well. Further, many rotational states are energetically accessible at even low collision energy, so the dynamical "resolution" of the rotational state distribution is high.

It is these expectations, substantiated by numerous experimental results, that propel this review. Rotations do indeed tell the tale.

As an aside, albeit an important one, we must explain the use of the term "rotational state", which obviously will appear repeatedly in this article. In use here, it means a particular value of a rotational quantum number, j', or a pair of rotational quantum numbers for a polyatom. This j', of course, specifies an energy level, not a unique quantum state. However accurate it would be, having to refer to vibrational states but rotational energy levels in any discussion of state-to-state experiments is awkward. We will term molecules having a particular value of j' as being in a particular rotational state, as it is clear that there is no misrepresentation implied and unlikely to be perceived.

Also, it is wise to acknowledge that none of the experiments described here are in the strictist sense state-to-state, meaning reaction taking place from one selected quantum state of the reactants. There is not one rotational quantum state of the reactants, not even one rotational energy level, but rather several. For the reaction of polyatomic species, there is even more than one vibrational state, because of the thermal population of low-frequency bending and torsion vibrations. However, the thermal distribution over reactant states, both vibrational and rotational, is not significant. The resultant distribution of energies and distribution of angular momenta are small compared to the total energy and the total angular momentum, which are set by the high collision energies of these experiments. We use the term state-to-state here just as it is used commonly in the field.

II. Methodology

The results described in this review are primarily experimental, but computational simulation also plays an important role. The experiments use the typical pump−probe approach under the single-collision conditions necessary to make state-to-state measurements meaningful.[2] The "pump," a UV laser pulse of a few nanosecond duration, initiates reaction at a well-defined time by photolysis of a precursor for one of the reactants. For example, photolysis of HI yields H atoms, and photolysis of Cl_2 gives Cl.[18] After a delay of typically a few tens of nanoseconds, a "probe", a second laser pulse, also of a few nanosecond duration, detects the reaction products, with electronic, vibrational, and rotational state selectivity. The time between the pump and probe pulses is chosen to be short enough that for the pressures of the reactants used the probability of more than one collision during this delay period is small.

The probe spectroscopy used in the experiments described here is resonant multiphoton ionization (REMPI)[19,20] or coherent anti-Stokes Raman scattering (CARS).[21,3] Each has advantages. REMPI has very high sensitivity but is limited in use to systems with well-characterized spectroscopy and readily accessible electronically excited intermediate states. CARS is universal, but lacks sensitivity. Its analysis allows absolute partial and total reaction cross sections to be determined, not just state distributions. Each method is well suited for some set of conditions that are important for state-to-state measurements.

Computations are used here to interpret the experimental measurements. State-to-state experiments generate very detailed and very abundant data. Interpretation of the data is needed to

illuminate the reaction dynamics and to produce the map of the reaction. This can come from a model description that accounts for the data in terms of a limited number of assumptions about the dynamics. However, when possible, computational simulation of the data can provide more insight and a much better map. The simulations discussed here are based on quasiclassical trajectory (QCT) calculations.[22] These are feasible and have been executed for several of the reactive systems that are described here.[23]

The state-to-state measurements provide a stringent test of the accuracy of the QCT calculations. When the computational results are confirmed by such detailed experiments, their validity, even outside the range of data on which they have been confirmed, is strongly supported. Because the trajectories can be followed in real time, they can be used directly to develop the map of the dynamics. They serve to peel back the cover on the black box in which the dynamics takes place.

III. Selected Results

Despite the importance of computational simulation, our effort in studying the dynamics of chemical reactions has aimed at providing descriptions that are general and classifying and therefore do not make reference to specific features of the potential energy surface for a particular system. In fact, we try to develop descriptions that do not require a knowledge of the full potential energy surface (PES) for a reaction yet still provide dynamical understanding. If the full PES is known from ab initio quantum chemistry, the dynamics can be reliably expressed by some quantum, semiclassical, or quasiclassical calculation. However, for any but the simplest chemical reactions, the full PES is so complicated that it is not easily obtained by ab initio methods. The problem is primarily one of the dimensionality of the surface.

The dimensionality of the PES is large enough to be problematic for many reactions that any chemist would surely consider very simple. For example, for $H + CH_4 \rightarrow H_2 + CH_3$, which is the simplest reaction at a carbon center, and among the simpler reactions that will be dealt with in this review, the PES is 12-dimensional. For calculation of the thermal rate constant, only information near the minimum energy path is needed, and the problem, although not trivial, is tractable. However, in state-to-state dynamics studies, geometries far from the minimum energy path are sampled, so the PES must be known over a large range of this 12-dimensional surface to be adequate to account for the dynamics. There are new methods that make this situation more tractable and are likely to facilitate more extensive computational exploration of polyatomic reaction dynamics in the future, but we live in the present.

So, our approach is to try to develop descriptions of the reaction dynamics that are expressable in terms of characteristics of the reaction system that are more readily accessible than the full PES. We have settled on a classification and explanation scheme in which the descriptors are kinematics, thermochemisty, and reactant structure. The last incorporates stereochemistry as well as simple geometrical structure. Understanding of the reaction dynamics in terms of these descriptors will never be as detailed as that which would come from a complete dynamics calculation on the full PES, but we believe that it can be sufficient to be useful. The readers can judge that for themselves, after having read this article.

A. Analysis of Product Rovibrational State Distributions. It may seem odd to begin this section with a discussion of analysis of results before any have been presented. However, we have found a general feature of the product state distributions

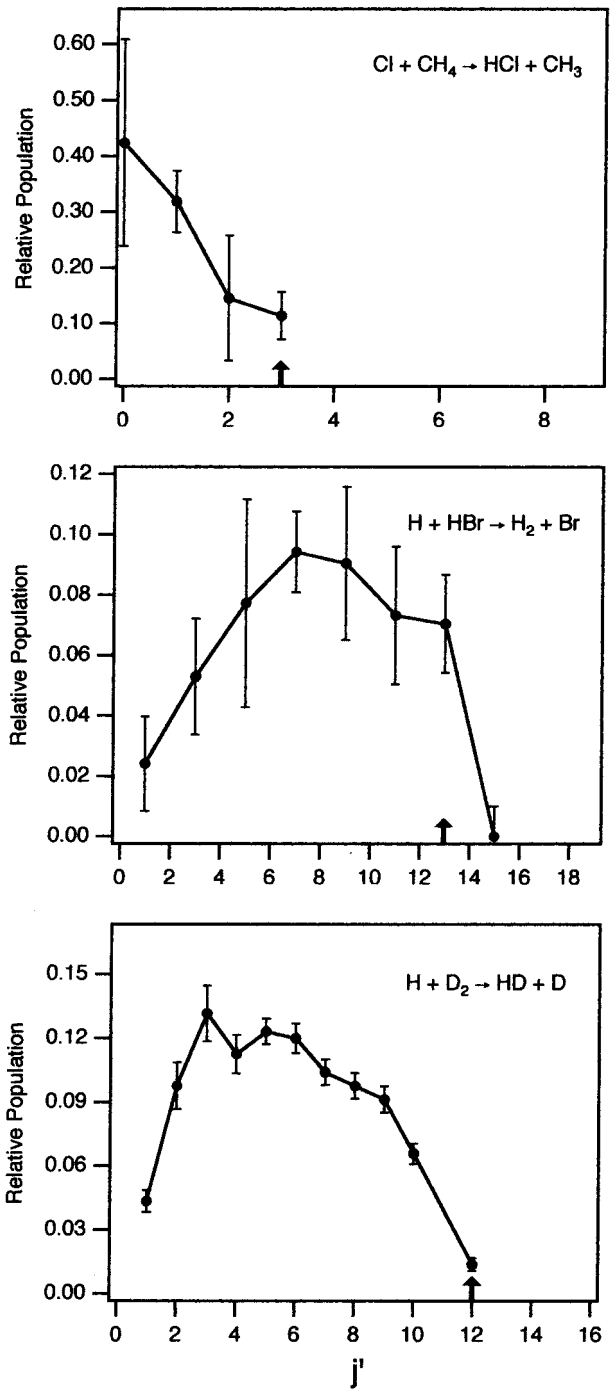

Figure 5. Rotational state distribution for the HCl, H_2, or HD $v' = 0$ product of the $Cl + CH_4$, $H + HBr$, and $H + D_2$ reactions, at collision energies of 0.2, 1.6, and 1.3 eV, respectively. The range of the rotational angular momentum axis extends to that value of j' that is the largest allowed by total energy conservation. The arrow on the axis indicates the largest value of j' for which product is observed.

that directs how these distributions should be presented and meaningfully discussed. Without getting too far ahead of the discussion, we will note that this general feature happens to express the influence of kinematics on the reaction dynamics, one of the three descriptors on which we have focused.

The dynamical behavior that lead to our finding the expression of kinematic effects can be illustrated by any of the large number of specific cases from which the generalization was subsequently drawn. Figure 5 shows the $v' = 0$ rotational state distributions for three reactions, $H + D_2 \rightarrow HD + H$,[14,15] $H + HBr \rightarrow H_2 + Br$,[3] and $Cl + CH_4 \rightarrow HCl + CH_3$,[24] plotted as probability versus

rotational quantum number. The rotational angular momentum axis extends out to the maximum j' allowed by total energy conservation, that is, to a value of j' for which the product rotational energy, E'_{rot}, is no more than the total available energy, E_{tot}, where $E_{tot} = E_{trans} + E_{int,\ reactant} - \Delta H_{reaction}$, where E_{int} reactant is the rovibrational energy of the reactants.

The highest observed value of j' is marked by the vertical arrow on the abscissa. In each plot, there is a region of j' space, to the right of the arrow, in which no population is observable. The region without population is small for H + D_2 → HD + H, a bit larger for H + HBr → H_2 + Br, and very large for Cl + CH_4 → HCl + CH_3. The behavior is the same if we look at rotational state distributions for $v' = 1$, in which case the maximum observed j' is below, sometimes well below, that allowed by $E'_{rot} = E_{tot} - E'_{vib} = E_{trans} + E_{int,\ reactant} - \Delta H_{reaction} - E'_{vib}$. A similar constraint that is more restrictive than total energy conservation is also observed for the vibrational state distributions. It seems that for rovibrational energy released to the products the energy that is actually available is generally less, sometimes much less, than the total energy.

We were intrigued by the generality of this observation, and we sought to explain it. We developed a model that quantitatively accounts for the restriction of product rovibrational state distributions to an energy less than the total energy, with the restriction being to a specific energy that is characteristic of each reaction. The model description has no adjustable parameters and consequently has predictive as well as explanatory power.[25] The model invokes the operation of a kinematic constraint on reactions at suprathreshold collision energies. State-to-state dynamics studies are generally done at suprathreshold collision energies, so the model pertains to a situation that is quite general.

The model has only one postulate, that at these collision energies direct atom transfer reactions occur by the trajectory reflecting off the inner corner of the potential energy surface in the (r_{AB}, r_{BC}) two-mathematical-dimension subspace of the surface that describes the bond breaking and bond making in A + BC → AB + C. From this one postulate it is easy to show that the product *translational* energy must be *greater than some minimum value* for the trajectory to be able to get from the reactant valley to the product valley. This comes about very simply if we represent this two-dimensional subspace in mass-scaled Jocobi coordinates to incorporate mass effects directly and then analyze the characteristics of reflections that will send the system on to products or back to reactants. Reflections that would lead to too little product translation cannot go on to products, but instead they come back out as reactants.

It is important to note that A, B, and C can be atoms, diatoms, or polyatoms, and the model is consequently applicable not only to atom transfer chemical reactions but also to reactions in which the transferred species is molecular.

The minimum bound on the product translational energy obviously implies a *maximum bound* on the product *internal energy*. We showed that the upper bound on the internal energy is given by

$$E_{effective} = \sin^2 \beta\,(E_{trans} - \Delta H) \qquad \text{(endothermic reactions)} \tag{1}$$

$$E_{effective} = \sin^2 \beta\,(E_{trans}) - \Delta H \qquad \text{(exothermic reactions)} \tag{2}$$

$$E_{effective} = \sin^2 \beta\,(E_{trans}) \qquad \text{(thermoneutral reactions)} \tag{3}$$

Here β is the skew angle,[2] $\beta = \arccos[m_A m_C/(m_A + m_B)(m_B + m_C)]^{1/2}$, for the reaction A + BC → AB + C, and it is the quantitative carrier of the kinematic influence on the reaction dynamics.

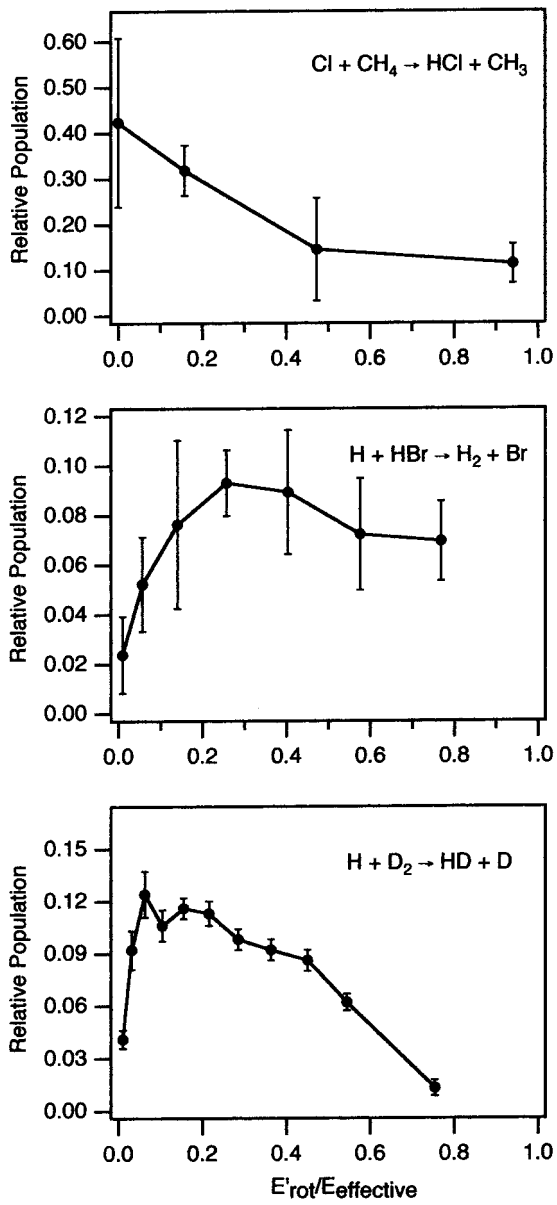

Figure 6. Rotational state distributions of Figure 5, now plotted as a function of rotational energy divided by the effective energy available to product rotation and vibration. See text for details.

A limiting value of β occurs for the kinematic combination heavy + light−heavy → heavy−light + heavy, for which β approaches 0° and the kinematic constraint is most severe. This is exemplified by the reaction I + HBr → HI + Br and also closely approximated by Cl + CH_4 → HCl + CH_3, for which we have presented data in Figure 5. The other limit is associated with the combination light + heavy−light → light−heavy + light, for which β approaches 90°, exemplified by H + DI → HI + D, and approximated by H + CO_2 → OH + CO.

The three state distributions of Figure 5 are replotted in Figure 6 on a reduced energy scale that explicitly incorporates the kinematically constrained $E_{effective}$. In each case, the measured distribution extends up to the maximum j' allowed by the constraint of the rovibrational energy to be no greater than $E_{effective}$. In each case, the next higher j' has an energy that exceeds $E_{effective}$; that is, it occurs at a value of greater than 1.0 in the reduced energy units of the figure.

We have examined data from all of the state-to-state dynamics studies that have been carried out. These include the reactions $H + H_2 \rightarrow H_2 + H$ and its isotopomers; $H + HX \rightarrow H_2 + X$ (HX = hydrogen halide), $H + RH \rightarrow H_2 + R$ (RH = alkane), and isotopomers; $H + H_2O \rightarrow H_2 + OH$ and isotopomers; $Cl + RH \rightarrow HCl + R$ (RH = alkane) and isotopomers. For all reactions for which the state-to-state data have been measured, the product rovibrational state distributions are quantitatively consistent with the predictions of the kinematic model. Occasionally there is population in a state just above the kinematic limit, when the kinematic limit is computed using the nominal total energy for the reaction, but this is because there is sometimes a spread in the total energy[26] that yields a spread in the kinematically constrained energy.

There are two other reactions for which complete rovibrational state distributions are known that bear mention here. The first is the $H + CO_2 \rightarrow OH + CO$ reaction. We have already mentioned that the mass combination in this reaction gives β near 90°. As eqs 1−3 show, for this value of β, there is no significant kinematic constraint. The OH rovibrational state distribution has been measured several times over a range of energies, all high because of the use of photolytic hot H atoms.[27−36] The results of these measurements show that essentially all states that are accessible at the total available energy are in fact populated. That this is consistent with the model is significant. The model's validity is just as supported when it correctly predicts no significant constraint, as when it correctly predicts a severe one. This is important in believing that we get the right result for the right reason.

There is also a reason the model might not even apply to this reaction. The model describes direct atom transfer reactions. For the $H + CO_2 \rightarrow OH + CO$ reaction, there is a strongly bound intermediate, HOCO,[37] and the reaction can take place through this complex. The model is not applicable to complex-forming reactions. However, the experimental studies of this reaction have been done at high energies for which reaction through the complex may not be important. Either way, the fidelity of the model is supported by the fact there is no kinematic constraint on the products of this reaction.

The one single exception to the model is also one that supports the conceptual basis of it. This is the $H + HCN \rightarrow H_2 + CN$ reaction. There are no experimental measurements of the H_2 product rovibrational state distributions for this reaction. However, there are detailed QCT calculations on this system that report such distributions.[38] The computed H_2 product rovibrational state distributions sample all of the range of v' and j' allowed by total energy conservation; there is no kinematic constraint, and there should not be one for this reaction. The kinematics of the reaction, light + light−heavy → light−light + heavy, lead to β near 45° and thus the potential for kinematic constraint. However, the nature of this reaction is one that is not covered by the model.

The model describes reaction as occurring by a trajectory reflecting off the inner corner of the potential energy surface in the two-dimensional configuration space of r_{AB} and r_{BC}, which for this reaction is r_{HH}, r_{H-CN}. (More correctly, it is the two-dimensional configuration space of the mass-scaled Jacobi coordinates derived from these bond coordinates.) For the H + HCN reaction, this is not how reaction occurs. Because this reaction is extremely endoergic, it has a saddle point very far into the product channel,[39] and whatever happens at the inner corner of the potential energy surface does not control reaction in the way that the model invokes. The transition state is nowhere near the corner of the potential energy surface, rather it will closely resemble the products.[40] So, it is the motion through this transition state, a motion that is mostly H−CN vibration, that drives the reaction.

The mechanism of the $H + HCN \rightarrow H_2 + CN$ reaction is different from the mechanism of our model, and so the model is not applicable. However, reference to this reaction is meaningful, as it demonstrates that in a case where the model is inoperative the constraint on the product rovibrational energy disposal is not observed. This also helps establish that the dynamical picture in the model is right; that is, it is the actual source of the rovibrational energy constraint. The constraint does not appear when it should not, that is, when the model is not operative, lending credence to the belief that the invoked dynamics are really the source of the empirically observed effect.

B. $H + HX \rightarrow H_2 + X$ (HX = HCl, HBr, HI) Reactions. These reactions form a homologous series in which the kinematics (light + light−heavy → light−light + heavy, $\beta \approx 45°$) are constant, but the thermochemistry varies greatly: $\Delta H_0 = -0.05$, -0.72, and -1.42 eV, for HCl, HBr, and HI, respectively.[4] So, they should be useful in elaborating the influence of the thermochemistry variable in the three-dimensional conceptual space of kinematics, thermochemistry, and reactant structure in which we attempt to classify and explain the dynamics. We have already seen in Figure 1 how this thermochemistry controls the H_2 vibrational state distribution, but the emphasis of this review, as well as the emphasis of our work, is on rotational state distributions. We will now look at these.

First, however, it is worthwhile looking at some actual experimental data. Unprocessed data from a state-to-state dynamics experiment is generally not very interesting to look at, or very informative for that matter. The data analysis is neither complicated nor difficult, but analysis is required before anything can be said about the experimental results. The data consist of spectra, in our work either CARS or REMPI spectra, of the $H_2(v',j')$ reaction product. The spectra are not continuous, but rather, they are composed simply of laser frequency scans over line profiles, the widths of which are due to Doppler broadening or instrumentally limited resolution. However, a review like this should show some "raw" data, and we do so in Figure 7, where we present the CARS spectra of $H_2(v',j')$ reaction product from the H + HI reaction.[3]

The spectra show the dispersive line shapes characteristic of CARS detection of species at low relative concentration.[21] Note however, that the phase of the line shape varies. This is due to the fact that the CARS method is detecting the $H_2(v',j')$ reaction product via a Q-branch $v' \rightarrow v'+1$ vibrational transition, and so it has a signal magnitude proportional to the population difference between states, $\Delta N = N(v',j') - N(v'+1,j')$. The H + HI reaction leads to $H_2(v',j')$ with vibrational population inversion for some $v',j'/v'+1,j'$ pairs, giving a negative value of ΔN and a signal line shape phase reversed from that for ΔN positive. Note also the segment of the CARS scan over the quantum state $v' = 1, j' = 7$. Here there is essentially no signal, despite the fact that there is considerable population in this quantum state. It just happens that $N(v' = 1,j' = 7)$ is very nearly equal to $N(v' = 2,j' = 7)$, giving ΔN near zero and, consequently, near zero signal.

Equivalent spectra from the experiments in which we use REMPI detection will not be shown. They are broad and featureless, varying little with v',j', and they have signal magnitudes that depend on the wavelength-dependent laser pulse energy and the transition-dependent line strength factors. As a

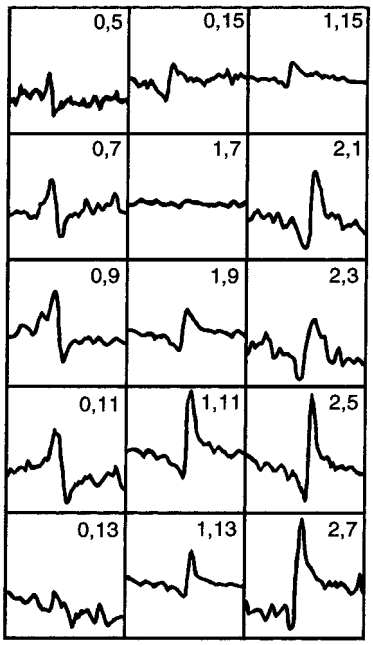

Figure 7. Representative CARS spectra of the $H_2(v',j')$ product of the H + HI reaction at 1.6 eV collision energy. The labels in the corner of each panel indicate v',j'.

consequence, they are both boring to look at and uninformative without full processing.

Figures 8−10 show $H_2(v',j')$ product rovibrational state distributions for the three H + HX reactions studied at a relative energy of 1.6 eV using H atoms produced by photolysis of HI.[3] Like the corresponding vibrational state distributions, these show the effect of reaction thermochemistry. However, they do so in much greater detail. They are plotted as a function of reduced rotational energy, using the kinematically limited available energy already discussed. It was in fact these reactions that first set us on the trail that led to the recognition of the kinematic limit.

We note here that there are actually two collision energies, 1.6 and 0.7 eV, in the experiments from which the data in Figures 8−10 was obtained. This occurs because the photolysis of HI in the UV yields both H + $I(^2P_{3/2})$ and H + $I^*(^2P_{1/2})$; in this specific case of 266 nm photolysis, the two channels are in a nearly 1:1 ratio.[41] H atoms of both energies contribute to the product yield, though the higher energy collisions dominate.[23] For the kinematic analysis, it is obviously appropriate to use the higher energy in calculating the kinematically constrained available energy. For comparison of QCT calculations with the experiments, we have done the calculations at both collision energies and combined the results to make the comparison meaningful. We have done other experimental and computational studies of the H + HX → H_2 + X reaction system under HI photolysis conditions that yield only one H + I fragment channel and thus a single collision energy.[42] These are not as extensive as our other experiments, and we will not discuss them, except to say that they support the conclusions we draw here.

What interpretation do we make of these distributions? The first pass at that comes from an information theoretic analysis.[2] This is an analysis that we have used consistently to characterize our rotational state distributions. In its linear surprisal expression with a single variable, the surprisal parameter, it represents the minimal energy analysis of an ensemble of products that have fixed total energy. There is no reason that a linear surprisal should fit the data, but in every case but one, it does. The

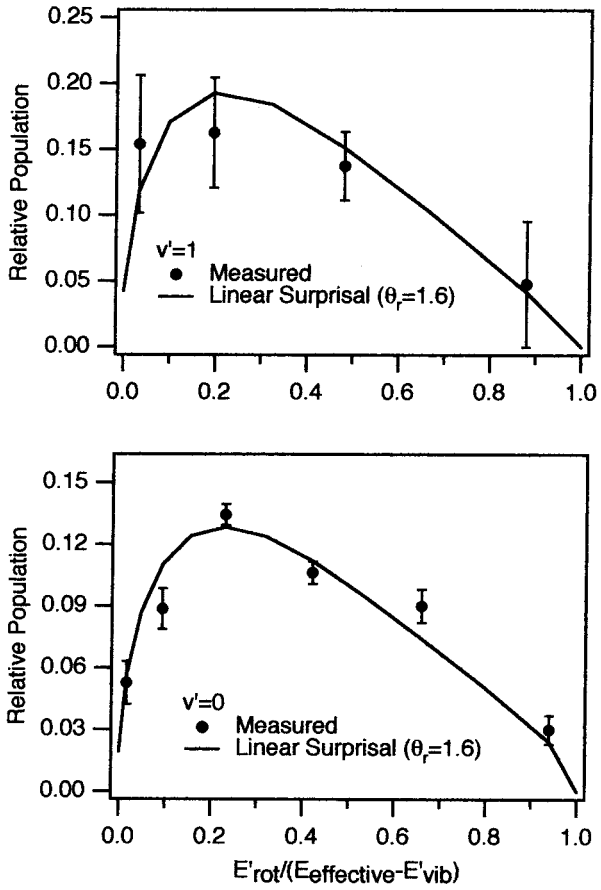

Figure 8. Rotational state distribution for the $H_2(v',j')$ product of the H + HCl reaction at 1.6 eV collision energy, plotted as a function of reduced rotational energy, using the effective energy available to product rotation/vibration. The symbols with error bars show the experimental results, and the curves give the best-fit linear surprisal representation of the data with the surprisal parameters indicated.

exception is H + HI. The surprisal fits to the data for the H + HCl and H + HBr reactions are shown as the solid curves in Figures 8 and 9.

The linear surprisal parameter, θ_R, comes from a fit of the expression

$$P(j';v') = P_0(j';v') \exp -[E'_{rot}(j';v')/(E_{effective}/\theta_R)] \quad (4)$$

where $P(j';v')$ is the observed normalized probability of forming H_2 product in state v',j', $P_0(j';v')$ is the full state degeneracy for product in v',j', $E'_{rot}(j';v')$ is the rotational energy, and $E_{effective}$ is the kinematically limited available energy. θ_R can be positive or negative and characterizes the average energy disposal into rotation for products in a particular v'.

As we can see from the figures, the surprisal parameters are all positive, indicating that less energy is partitioned to product rotation than would be the case if each unique quantum state were populated equally, that is, without dynamical "bias." For the thermoneutral H + HCl, the rotational surprisal parameter is the same for products in $v' = 0$ and$'$ 1. This is the same as what is observed for H + D_2. In contrast, for H + HBr the rotational surprisal parameter increases as v' increases, indicating that this bias increases with increasing energy in product vibration. These are characteristic features of the H + HX reactions that stand in contrast to the behavior for the H + RH (RH = alkane) reactions that we will discuss in the next section.

The linear surprisal analysis characterizes the rotational state distribution as being controlled by a single dynamical constraint,

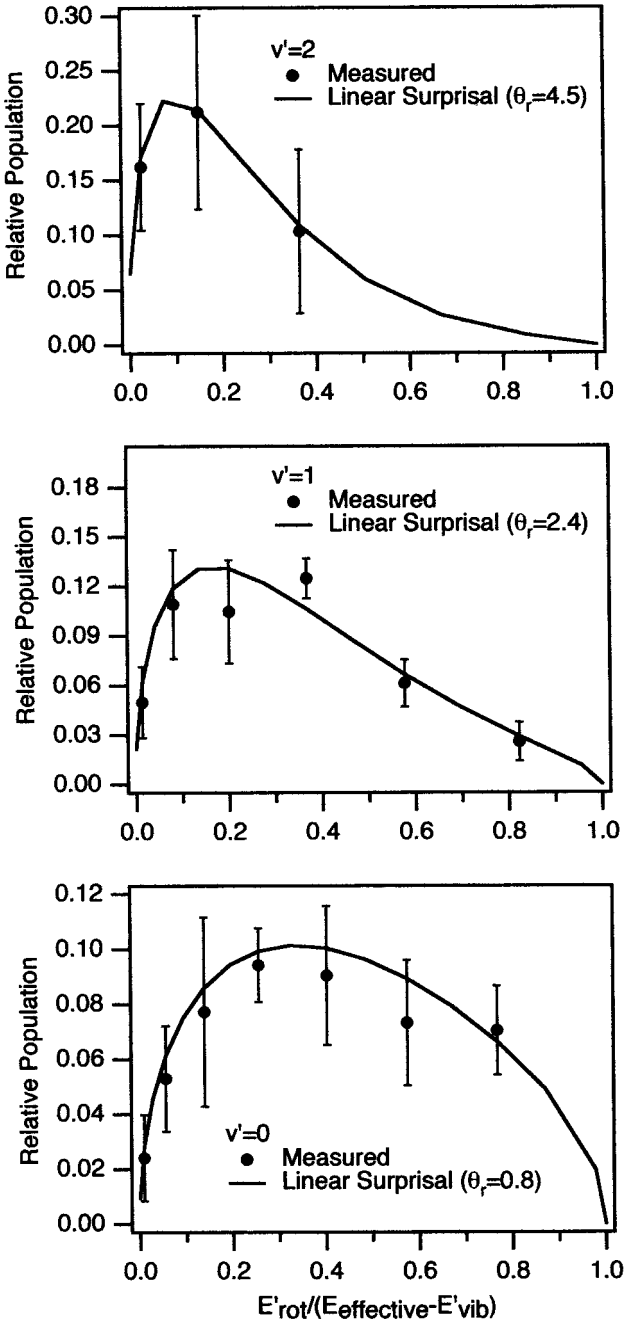

Figure 9. Rotational state distribution for the $H_2(v',j')$ product of the H + HBr reaction at 1.6 eV collision energy, plotted as in Figure 8.

quantitatively represented by the surprisal parameter. There is no reason this should work. There are at least two constraints on the state distributions, because of conservation of total energy and conservation of total angular momentum. Furthermore, we know that there is a kinematic constraint. In fact, when we use the total available energy in the surprisal analysis, the linear surprisal description of the data is frequently not very good. This is the case with H_2 from H + HBr. However, a linear surprisal description works, as Figure 9 shows, when we use the kinematically constrained available energy.

What this tells us is that the kinematic constraint is the important energy constraint, not total energy conservation. In addition, it says that the remaining constraint, the one carried by the surprisal parameter, must be due to angular momentum conservation. The local reaction model that we describe below invokes angular momentum conservation control of the H_2 rotational state distribution and supports this conclusion.

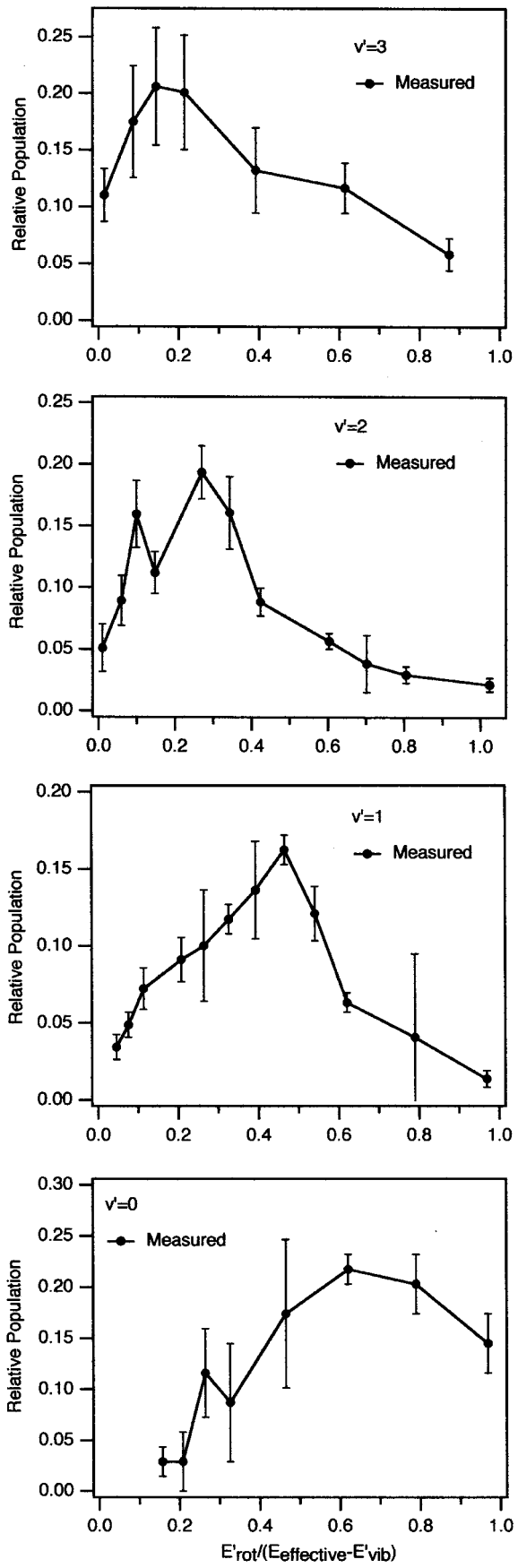

Figure 10. Rotational state distribution for the $H_2(v',j')$ product of the H + HI reaction at 1.6 eV collision energy, plotted as a function of reduced rotational energy as in Figures 8 and 9. The symbols with error bars are the experimental results, here the lines simply connect the data points.

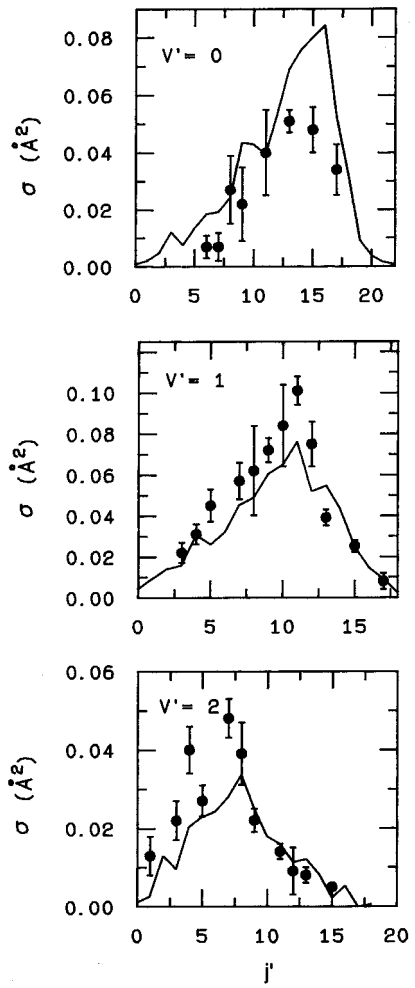

Figure 11. Comparison of experimental partial cross sections, shown as symbols with error bars, and partial cross sections computed from QCT calculations, shown as a line, for the $H_2(v',j')$ product of the H + HI reaction. The experimental data are derived from the results shown in Figure 10. Error bars on the QCT data have been removed to make the comparison clearer.

The second, more detailed, pass at interpreting the product rotational state distributions comes via the QCT calculations.[23] For each of the three H + HX reactions, fairly accurate potential energy surfaces have been developed, and the high (1.6 eV) collision energies make a classical description of the dynamics promising. This promise is realized, as a comparison of calculated and measured rovibrational state distributions shows. For all three reactions, the comparison shows excellent agreement. The most extensive comparison is obviously that for H + HI, given the large number of quantum states populated, and for that reason, we show it for three of the four v' observed in Figure 11. We note here that the comparison of Figure 11 involves no scaling, but it is a comparison of absolute partial cross sections that are computed and absolute partial cross sections that are measured. Being able to get absolute partial cross sections, not just product state distributions, is a hallmark of the CARS measurements of reaction products.

The level of agreement is sufficiently high that we have used the QCT calculations to interpret the dynamics, developing an understanding of the dynamics within the "black box" of the reaction. The analysis leads to a model of the reactions that not only describes the H + HX reactions but also forms the basis of a model for the H + RH (RH = alkane) reactions.

The model is compact and as easy to understand as it is to present. Its key feature is a "local" impact parameter, which

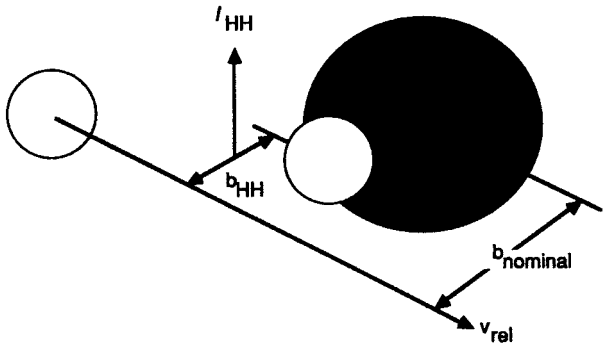

Figure 12. Schematic representation of a collision of H with HX, showing how the local impact parameter and associated angular momentum are defined.

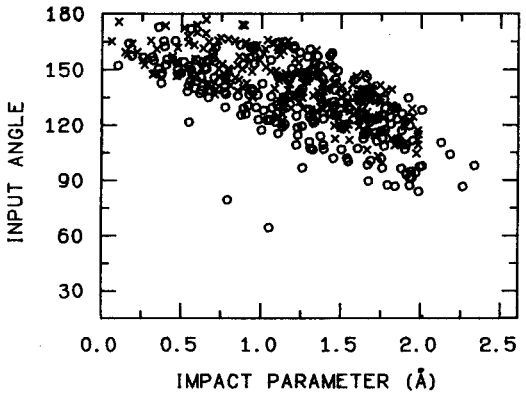

Figure 13. Scatter plot of the values of the input angle (angle between the relative velocity vector and the HCl axis) and impact parameter in reactive collisions of H + HCl to yield H_2. Each point represents a single reactive trajectory; those indicated by "o" are for reaction at 1.6 eV collision energy, and those indicated by "x" are for reaction at 0.7 eV. The angle 180° corresponds to collinear H−H−Cl input angle.

we call b_{HH}, that is, the distance between the relative velocity vector and a line parallel to it that passes through the H atom on the HX reactant. This is shown in Figure 12. The normal impact parameter, $b_{nominal}$ in the figure, refers to the distance between the relative velocity vector and a line drawn parallel to it that passes through the center-of-mass of the HX reactant. The diagram shows how the nominal impact parameter is of limited use for describing the collision properties that will influence the outcome of the reaction. The local impact parameter is intuitively appealing, because in these reactions it is the H atom of the HX that is reactive, and the close approach of the two H atoms is necessary for reaction. The diagram also shows a local orbital angular momentum, $l_{HH} = \mu_{HH} v_{rel} b_{HH}$, that is connected with this local impact parameter. This local impact parameter will become even more important when we discuss the H + RH (RH = alkane) reactions, for which the impact parameter with respect to one particular H atom of RH is key to describing the reaction.

Our use of the local impact parameter rests on much more than intuitive appeal. We found a strong correlation between the nominal impact parameter and the angle between the relative velocity vector and the H−X axis, which we call the input angle. This is illustrated by the input angle−impact parameter scatter plot for the H + HCl reaction in Figure 13. Each symbol represents one reactive trajectory. The correlation is such that for reactive trajectories the nominal impact parameter and the input angle must be matched to make the local impact parameter small. Further analysis of the trajectories shows that this local impact parameter not only determines if reaction will occur but also determines the rotational angular momentum of the H_2

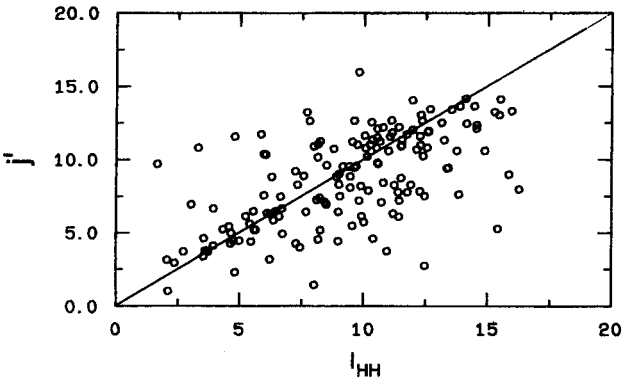

Figure 14. Correlation between the local orbital angular momentum, l_{HH}, and the rotational angular momentum of the H_2 product, j', in the H + HBr reaction. Each point represents a single reactive trajectory at 1.6 eV collision energy.

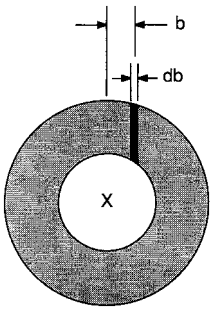

Figure 15. Shell model for the reaction H + HX → H_2 + X. The shaded annulus represents the ensemble of locations of the H atom of HX, whereas *b* is the impact parameter.

product. That is based on a strong correlation between j' and the local orbital angular momentum, l_{HH}. This is shown by the $j'-l_{HH}$ scatter plot in Figure 14 for the H + HBr reaction. These are the only correlations that emerged from a very detailed search within the trajectory results.

We call this description of the reaction the local reaction model, to indicate the importance of parametrization of the reaction dynamics in terms of measures of the interaction and approach of the two species that will be bound together to make the product molecule. This model is further supported by its ability to rationalize the opacity function for these reactions.

Its expression in this regard is the shell model, depicted in Figure 15. We represent the ensemble of orientations of the H atom of HX with respect to the relative velocity vector as an annulus, a shell, of uniform H atom probability distribution surrounding the halogen atom X. The size of the shell, given by the inner and outer radii, has to be specified to make this quantitative. We take the size to be given by the H−H and H−X distances at the saddle point of the potential energy surface.

The normal opacity function, the opacity as a function of the nominal impact parameter, *b*, not the local impact parameter, b_{HH}, is, in this shell model, the value of the line integral through the shell of H atom probability at a given value of *b*. The resultant H + HX opacity function, for H + HI, is shown in Figure 16, along with the opacity function from the QCT calculations. The agreement is quite good, given that there are no adjustable parameters in what is a very simple model. The model reduces the reaction probability to a simple stereochemistry that is purely geometric, without any steric effect, that is, without any dependence of interaction energy on H−H-X geometry. This is of course not correct, but the model works well nonetheless. The agreement of the shell model and the QCT opacity function is better for H + HBr and a little worse for H + HCl.

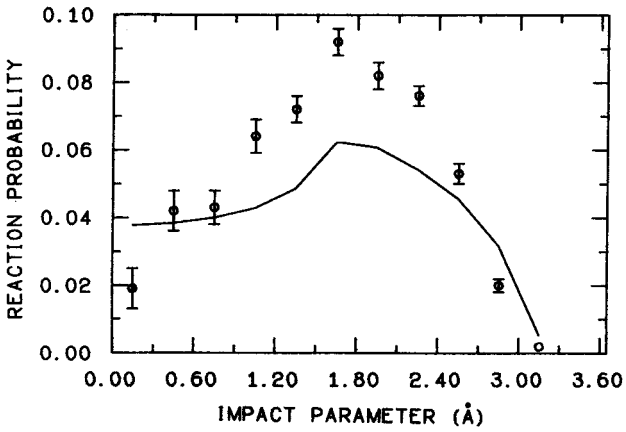

Figure 16. Comparison of the opacity function computed from QCT calculations, shown as symbols with error bars, and the opacity function predicted by the shell model, shown as the solid line, for the reaction H + HI → H_2 + I.

So this reaction model successfully accounts for all aspects of both our experimental measurements and computational simulations on the H + HX → H_2 + X reactions. It draws a clear map of these reactions with a quite localized and specific path taken by the attacking H atom and the abstracted H atom to make the H_2 product. The important features of the path and the map are clear in the local opacity function and the shell model.

This model, built on the simple H + HX atom−diatom system plays a central role in explicating the dynamics of the H + RH → H_2 + R (RH = alkane) reactions. For these, like H + HX, there is a local interaction between the attacking H and the abstracted H of RH, but this is modified by the presence of multiple local interactions resulting from multiple sites for H atom abstraction. For those reactions, we extend the local reaction model to account for the multiplicity of sites in a way that incorporates the stereochemisty of the RH reactant. In so doing, we explore the reactant structure element of our three-conceptual-dimension space of thermochemistry, kinematics, and structure.

C. H + RH → H_2 + R (RH = Alkane) Reactions. Like the H + HX → H_2 + X reactions, these alkane reactions form another homologous series. Like the H + HX reactions, they all have light + light−heavy → light−light + heavy kinematics with β near 45°. Their energetics are bracketed by the thermochemistry of the H + HCl and H + HBr reactions, as they are nearly thermoneutral to mildy exoergic, depending on the identity of RH. For a given alkane, the thermochemistry is also dependent on the identity of the H atom that is abstracted, the obvious, though not only, part of which is whether it is a primary, secondary, or tertiary H. The more subtle distinctions among the H atoms within and between RH do play a role.

State-to-state dynamics at the level described here involves the measurement of only scalar quantities. In the absence of measured vector quantities, it might seem that steric and dynamical stereochemistry effects would be inaccessible. Although the probing of them is indirect, it does appear that the influence of steric and stereochemical forces can be felt in the state-to-state cross sections. It is the rotational state distributions that are important, just as they were in expressing the stereochemical effects in the H + HX reactions that serve as benchmarks for interpretation of the H + RH reactions. The rotational state distributions are what distinguish one reaction from another and, hence, reveal the characteristic dynamics.

These rotational state distributions make sense and become interpretable when the complete set of them are analyzed as a

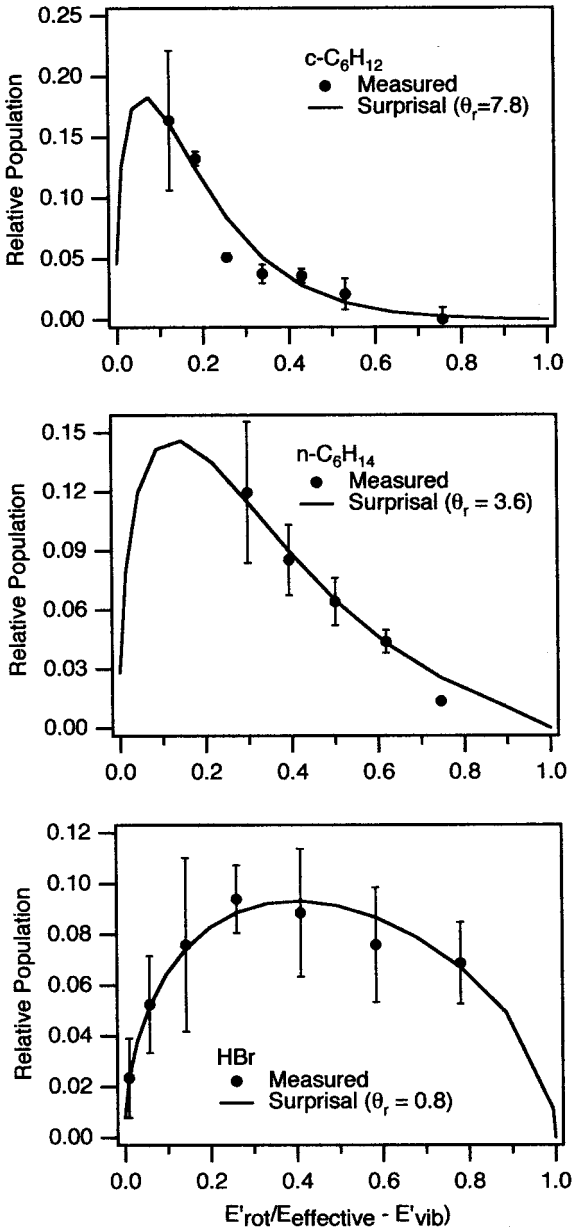

Figure 17. $H_2(v' = 0,j')$ product rotational state distributions for the reaction of H with *c*-C_6H_{12}, *n*-C_6H_{14}, and HBr, at a collision energy of 1.6 eV, plotted as a function of reduced rotational energy. The symbols with error bars are the experimental results; the solid curves give the best-fit linear surprisal function representation of the experimental data with the surprisal parameters indicated.

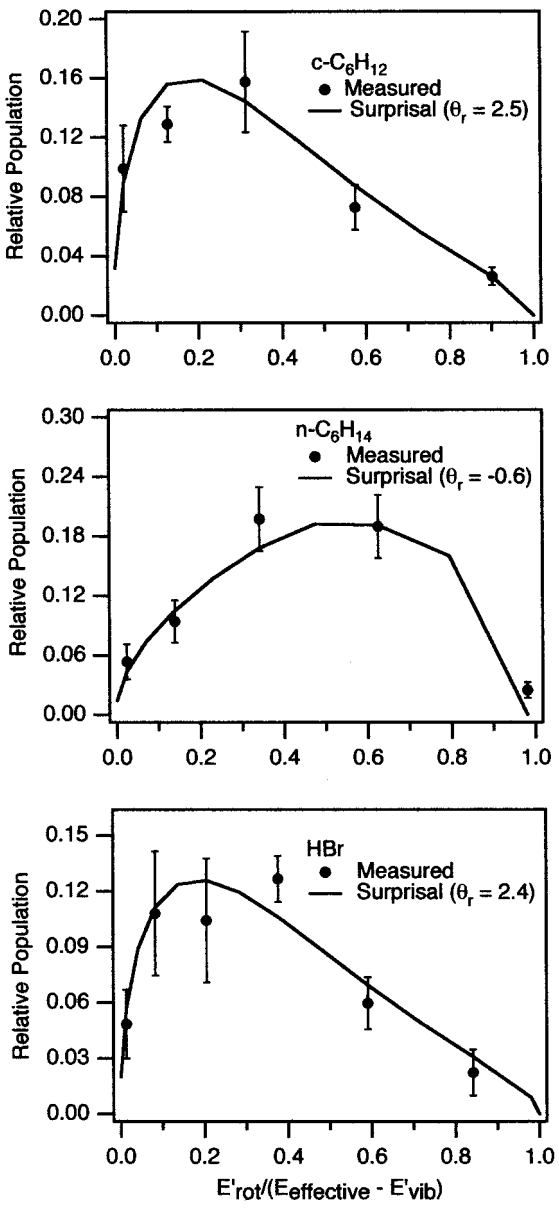

Figure 18. As in Figure 17, but for the $H_2(v' = 1,j')$ product.

whole body, rather than as a series. We start this with the data comparison shown in Figures 17 and 18, where we plot the rotational state distributions for H + HBr,[3] H + *n*-hexane,[43] and H + cyclohexane[17] reactions in $v' = 0$ (Figure 17) and $v' = 1$ (Figure 18). These plots, like others we have shown, are done in reduced-energy space using the kinematically constrained available energy. The solid curves in the plots are best-fit linear surprisals, using eq 4, which we find faithfully represent the data. The surprisals are sufficiently good fits that in some subsequent plots we will show only the surprisals and not individual data when making comparisons to illustrate trends within the results.

It is important to point out here that linear surprisal description of the H + RH $\rightarrow$ $H_2(v',j')$) + R product rotational state distributions is not good if we use the total available energy in the surprisal analysis of eq 4. However, when we use the kinematically constrained available energy, the linear surprisal representation is so good that it fits all of the data from all of the reactions perfectly. As we pointed out in the previous section, we interpret this to mean that the energy constraint on H_2 rotation results not from total energy conservation but rather from the more restrictive kinematic control. Then the linear surprisal analysis is simply carrying the effect of angular momentum conservation.

Figures 17 and 18 show that the rotational state distributions are characteristic of specific RH reactants. However, there is one behavior here that is shown in every H + RH reaction, a behavior that distinguishes this series of reactions from every other class of reactions for which state-to-state measurements have been made: the H + RH reactions have a unique positive correlation of H_2 product rotational and vibrational energy, what in short-hand we call the positive v',j' correlation. That is, the rotational energy of the products increases as the vibrational energy does. All other reactions that we know of have either no correlation, rotational and vibrational state distributions independent of one another, or a negative correlation, rotational energy decreasing with increasing vibrational energy.

TABLE 1: Rotational Energy Disposal in H + RH → H_2 +R Reactions

	reaction							
	H + CD_4	H + C_2H_6	H + C_3H_8	H + *n*-C_5H_{10}	H + *n*-C_6H_{14}	H + *c*-C_4H_8	H + *c*-C_5H_{10}	H + *c*-C_6H_{12}
E_{eff} (eV)	1.0	0.9	1.0	1.0	1.0	1.1	1.1	1.2
$\theta_t(v' = 0)$	5.0	4.2	4.1	3.8	3.6	4.6	8.0	7.7
$\theta_t(v' = 1)$	1.7	2.0	1.0	-0.4	−0.6		3.0	2.5
$\langle E'_{rot}(v' = 0)\rangle/(E_{eff} - E'_{vib})$	0.19	0.21	0.21	0.23	0.23	0.20	0.12	0.13
$\langle E'_{rot}(v' = 1)\rangle/(E_{eff} - E'_{vib})$	0.36	0.33	0.39	0.48	0.48		0.25	0.26

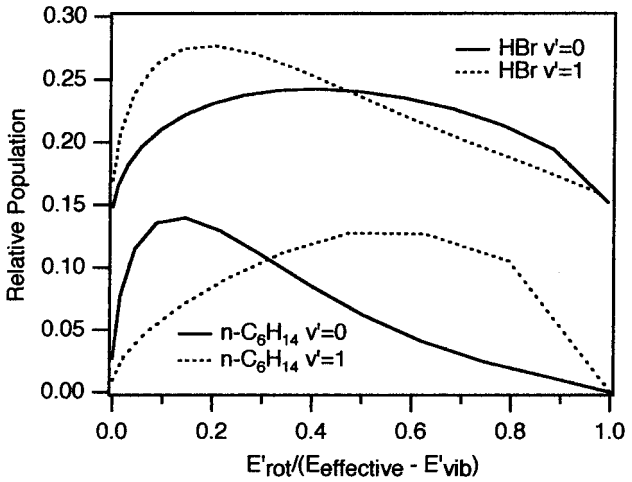

Figure 19. Comparison of the $H_2(v',j')$ product rotational state distributions for the H + HBr and H + *n*-C_6H_{14} reactions, plotted as a function of reduced rotational energy. Solid line, for $v' = 0$, and dashed line, for $v' = 1$, give the best-fit linear surprisal description of the data from Figures 17 and 18.

This can be easily seen qualitatively in Figures 17 and 18 by the shape of the rotational state distributions for H + *n*-hexane and H + cyclohexane reactions and the contrasting typical behavior for H + HBr. For $v' = 1$, both alkane distributions extend out to higher energies than in $v' = 0$, and for *n*-hexane, the $v' = 1$ distribution actually peaks at much higher energy. The behavior can be quantitatively gauged by the associated surprisal parameters. For cyclohexane, the $v' = 0$ value is 7.8, whereas the $v' = 1$ value is only a third of that at 2.5. For *n*-hexane, the $v' = 1$ surprisal parameter is not only smaller than that for $v' = 0$, it is actually near zero, a result that indicates that the $v' = 1$ rotational distribution is nearly statistical.

It is easiest to absorb the degree of this difference between H + RH reactions and all others, by the comparison in Figure 19. Here we have both $v' = 0$ and′ 1 for both the typical reaction (H + HBr)[3] and the exceptional H + RH (H + *n*-hexane)[43] in the same panel. Only the best-fit surprisal functions are shown; to include the four sets of data (Figures 17 and 18) results in visual congestion and an unreadable graph.

This is the appropriate place to make a note about the surprisal analysis[2] we use for the H + alkane reactions. We treat the alkyl radical as structureless for the analysis. We do this for three reasons, two fundamental and one practical. The first fundamental reason is that these H-by-H abstraction reactions take place on a very fast time scale, of the order of 10 fs.[44] This time is far too short for the heavy (relatively) C atoms to follow, and even too short for most of the hydrogenic vibrations, so almost all of the radical vibrations are dynamically inaccessible. The second fundamental reason is closely realated: these are direct and localized reactions in which almost all of the alkane reactant is nonparticipatory, a spectator to the reaction. So, it would not be appropriate to treat all of the alkyl radical product modes as involved in the reaction, which is what a full surprisal analysis would do. The practical reason for not treating them is a very simple one. To do a full surprisal analysis, we need to know the energy level structure of the alkyl radical product up to the 1.5−1.9 eV total energy of the reaction. This data is simply not available.

We use the surprisal parameters almost exclusively in a relative sense, to compare reactions to one another, all analyzed in the same way, with the parameters carrying in compact form the average energy disposal. This interreaction comparison is not likely to be invalidated by using this reduced dimensionality surprisal. The use of the reduced dimensionality analysis does provide the context for statements such as the one made just above that a near zero surprisal parameter for $v' = 1$ in the reaction H + *n*-hexane means that the rotations are populated nearly statistically.

If we accept the interpretation that the linear surprisal parameter is carrying the effect of angular momentum conservation (vide supra), then the near zero value of the surprisal parameter for $H_2(v' = 1,j')$ from H + *n*-hexane, and also H + *n*-pentane, is very important. It means that there is effectively no angular momentum constraint on the $H_2(v' = 1)$ product from these reactions. This is the limiting case of the local reaction model as extended to the H + RH reactions (vide infra). That extension takes account that the coproduct of H_2 is a polyatom with large moments of inertia that allow the rotation of the alkyl radical product to compensate the rotational angular momentum of the H_2 at almost no "cost" in energy. In the limiting case it allows the total angular momentum to be conserved for any for almost any H_2 rotational state.

The average energy disposal results for several of the H + RH reactions that we have studied and analyzed to date are shown in Table 1 in terms of both the surprisal parameters and the more conventional average energies. The positive v',j' correlation is always present, even though the average rotational energy disposal varies considerably with the identity of RH.

Figures 17 and 18 obviously give a small look at that in comparing the reaction of *n*-hexane with cyclohexane, but let us look at that variation in a systematic way. First, we observe that the $v' = 0$ rotational state distributions are the same for all linear alkanes.[16,17,43,45−47] In contrast, the $v' = 1$ rotational state distributions get warmer as the length of the alkane chain increases, though this trend seems to "saturate" at C5, because *n*-pentane and *n*-hexane are indistinguishable. These two features can be seen in the average energy disposals collected in Table 1, and more clearly in Figure 20.

We have fewer examples of reactions of cyclic alkanes.[17,47] This is the location of our present experiments, which are not yet complete. However, as for the linear C5 and C6 alkanes, the corresponding cyclic alkanes behave identically. There is a difference between the smaller cyclic alkanes, cyclopropane and cyclobutane, and the larger ones, cyclopentane and cyclohexane. Cyclopropane really is in a class by itself, as its electronic and molecular structure is quite different from that of the larger cyclic alkanes, and in fact, we do observe that it has a dynamical behavior all its own.[48] It is sufficiently different that it will not be included in this review. Cyclobutane does belong here, but we have data only for $v' = 0$, as the sample, which we had to

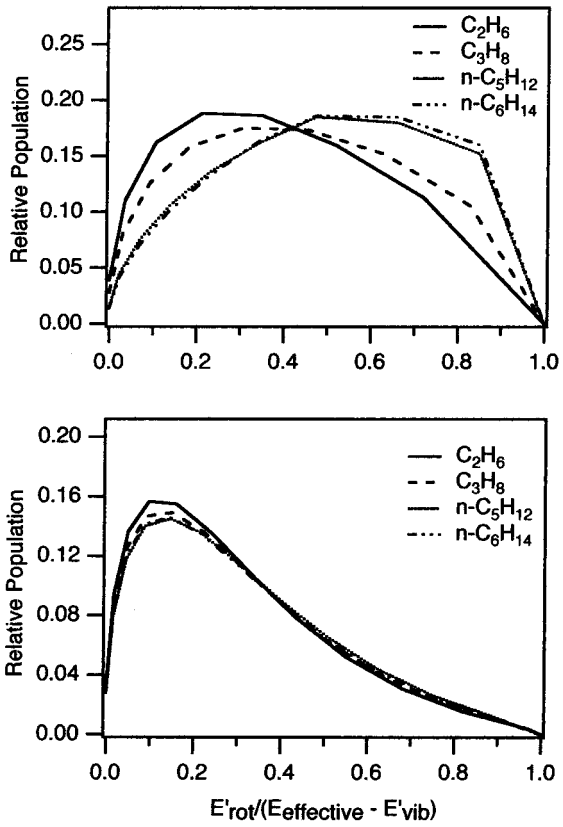

Figure 20. $H_2(v',j')$ product rotational state distributions for the reactions H + C_2H_6, H + C_3H_8, H +*n*-C_5H_{12}, and H + *n*-C_6H_{14},plotted as a function of reduced rotational energy. Top panel for $v' = 1$, bottom panel for $v' = 0$. The lines give the best-fit linear surprisal description of the data, with the surprisal parameters shown in Table 1.

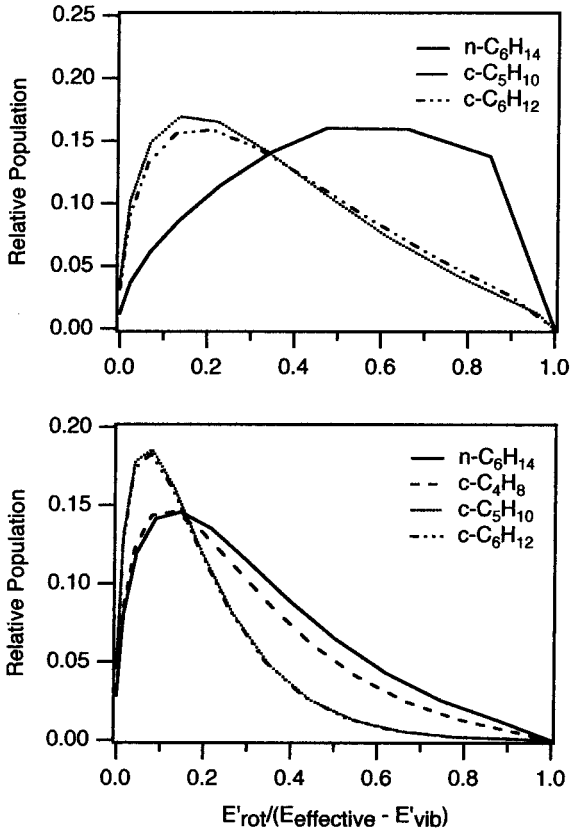

Figure 21. As for Figure 20, but for the reactions H + *n*-C_6H_{14}, H + *c*-C_4H_8, H + *c*-C_5H_{10}, and H + *c*-C_6H_{12}.

synthesize, was too limited to make it possible to complete measurements for $v' = 1$. So, Figure 21 shows what we do have to compare, and Table 1 compiles it.

Even with this admittedly limited cycloalkane data set there is enough to do some analysis. Clearly, the cyclic C5 and C6 alkanes behave quite differently from their linear analogues: they produce $v' = 0$ and $v' = 1$ rotational state distributions that are both colder, by a lot, than the $v' = 0$ and $v' = 1$ of the linear alkanes. Cyclobutane in contrast is, at least in $v' = 0$ where we have the data, nearly identical to the linear alkanes.

How to make sense of this? We start with the local reaction model that we built for the H + HX reactions, a model that successfully accounts for the observables, in both the experimental measurements and in the QCT calculations. Then we adapt it to incorporate the features that the H + RH reactions have that the H + HX do not: the presence of multiple H atom reactant sites and a polyatomic coproduct. The expanded local reaction model posits two effects of these features.[17,43,46,47]

The first effect in the model description is a truncation of the local opacity function caused by overlap of individual opacity functions on adjacent CH reaction sites. This is described by the molecular structures in Figure 22. Each circle represents the range of the local reactive opacity function centered on a particular CH group. Many collisions will fall within two (or sometimes three) of these circles, meaning that reaction with two (or sometimes three) CH's is possible, one with a larger impact parameter and another with a smaller impact parameter. Reaction at the smaller impact parameter is more probable, and in the aggregate, this leads to a reduction in reaction at the large impact parameter and a gain at the small impact parameter. This is what we mean by a truncation of the opacity function. In the

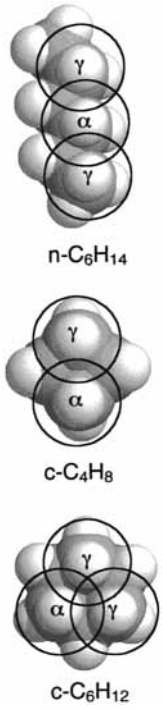

Figure 22. Schematic representation of the overlap of local opacity functions on neighboring C−H groups in three representative alkanes.

local reaction model of these reactions, the rotational angular momentum of the H_2 product correlates with the local orbital angular momentum, which is set by the local impact parameter. So, a truncation in the opacity function causes a reduction in H_2 product rotational angular momentum.

The second effect specific to the H + RH reactions that the model posits is associated with the presence of the polyatomic

coproduct. That leads to a relaxation of constraints on the H_2 product angular momentum, a relaxation made possible by the low-energy rotations in the alkyl radical. The involvement of the alkyl radical angular momenta make the constraints on H_2 product rotation due to conservation of total angular momentum less severe than when the coproduct is atomic. In addition, they relax the coupling between the total energy conservation and total angular momentum conservation relations, a coupling that further restricts the H_2 product rotation.

We can see how this works by considering the conservation relations. Let's look first at the H + HX → H_2 + X atom + diatom reactions:

$$E = E'_{\text{trans}} + E'_{H_2,\text{rot}} + E'_{H_2,\text{vib}} \quad (5)$$

$$\boldsymbol{J} = \boldsymbol{l}' + \boldsymbol{j}'_{H_2} \quad (6)$$

or by expanding the momentum and energy quantities:

$$E = {}^1/_2\mu' v'_{\text{rel}}{}^2 + hcB_{H_2}j'_{H_2}(j'_{H_2}+1) + hc\omega_{H_2}(v'_{H_2}+1) \quad (7)$$

$$\boldsymbol{J} = \mu' v'_{\text{rel}} b' + \boldsymbol{j}'_{H_2} \quad (8)$$

Here v'_{el} is the product relative velocity and B_{H_2} and ω_{H_2} are the H_2 rotational and vibrational constants. These two realations are tightly coupled because there are only two angular momenta and both appear in both relations. As a consequence, the H_2 product ends up significantly constrained by both the total angular momentum and the total available energy. With only two components, the angular momentum relation alone is quite restrictive, particularly because v'_{rel} is so high.

The situation with the H + RH → H_2 + R atom + polyatom reactions is quite different:

$$E = E'_{\text{trans}} + E'_{H_2,\text{rot}} + E'_{H_2,\text{vib}} + E'_{\text{R,rot}} \quad (9)$$

$$\boldsymbol{J} = \boldsymbol{l}' + \boldsymbol{j}'_{H_2} + \boldsymbol{j}'_{\text{A}} + \boldsymbol{j}'_{\text{B}} + \boldsymbol{j}'_{\text{C}} \quad (10)$$

where we have written the angular momentum of the radical product classically to emphasize its presence. Here we have neglected vibrational excitation of the alkyl radical for the same reasons we neglected including it in the surprisal analysis. However, its inclusion would change nothing in the model. Because the radical has large moments of inertia, even large values of $j'_{\text{A}} + j'_{\text{B}} + j'_{\text{C}}$ produce relatively small values of $E'_{\text{R,rot}}$, at least on the energy scale of these reaction studies. The last term in eq 9 then can be small compared to the other terms. So, the three alkyl radical angular momenta in eq 10 are not so important in eq 9. This partially decouples the energy and angular momentum conservation equations.

The extent of the decoupling depends on the magnitude of the moments of inertia of the radical. The impact of the decoupling is to make higher rotational states of H_2 product more accessible. The presence of the three alkyl radical angular momenta make higher j'_{H_2} accessible by providing more combinations of angular momenta that satisfy the total angular momentum conservation relation. Furthermore, they do this without any significant impact on the energy conservation relation.

Now we cannot make this model quantitative because to do so we need to know the shape and extent of the local opacity function, to which we have no independent access. We also need to know something about how the rotations of the radical and the rotation of H_2 are simultaneously engaged as the prodcuts separate, again inaccessible. So we also cannot make the model predictive. However, the model accommodates and can rationalize all of our observations about the rotational energy disposal in the H + RH reactions.

The two facets of the model, angular momentum constraint relaxation/decoupling and opacity function truncation, have opposing effects. One enhances rotational excitation of the H_2 product, whereas the other diminishes it. The truncation effect should be more important for $v' = 0$ products than for $v' = 1$ products, as the former comes from collisions that extend out to larger impact parameter than the latter.[44] The angular momentum effect should be larger for $v' = 1$ products than $v' = 0$ for the same reason. It can be engaged only if angular momentum can be transferred to the alkyl radical as the products separate, which is more likely as the impact parameter becomes smaller. So, the model description provides a way to understand the characteristic and distinguishing feature common to all of the H + RH reactions, that the $v' = 1$ products have a larger fraction of the available energy in rotation than do the $v' = 0$ products.

The model can also account for the differences among the different alkane reactants. Consider the differences between the linear and cyclic C5 and C6 alkanes, making reference to Figure 22. For the cyclic alkanes, the ring structure pulls adjacent CH groups closer together. This should make the opacity function truncation more pronounced and lead to colder rotational state distributions than those for *n*-pentane and *n*-hexane. Table 1 shows that this is indeed the case. In the case of cyclobutane, the overlap of the opacity functions should be about the same as in the linear alkanes, and so the fact that it has rotational energy disposal like the linear alkanes is, within the context of the model, sensible.

The trend within the series of linear alkanes is also understandable in the model. As the alkane radical gets longer, its moments of inertia get larger, making the decoupling of the conservation equations more effective. Also, it is easier to impart angular momentum to the radical as the lever arm on the radical increases, as it does as it gets longer. The rotational state distributions in both $v' = 0$ and $v' = 1$ get hotter (see Table 1) as the length of the alkane increases. The effect is stronger for $v' = 1$ than for $v' = 0$, consistent with the model description that the angular momentum relaxation and decoupling is more important for $v' = 1$ products than $v' = 0$.

The map for these H + RH → H_2 + R reactions is fuzzy, not sharp and focused like that for the simpler H + HX → H_2 + X reactions, because it is based on less information. However, it does suggest important features of the map of the reaction path map that are reasonable and can account for the experimental observations. It introduces two concepts, overlapping opacity functions and angular momentum constraint relaxation, that undoubtedly will play a role in a more detailed map to be drawn in the future.

IV. Conclusion

Through an examination of the results of state-to-state dynamics studies done in our laboratory, we have attempted to show how the measurement of rotational state distributions can provide some features of the map that directs the reaction system from reactants to products. The map is incomplete and the tale is an unfinished one, but we believe the first is useful and the latter interesting.

Acknowledgment. This work is supported by a grant from the U.S. Department of Energy. The author thanks David Danese and Nicholas Shuman for assistance in preparing this article.

References and Notes

(1) Weston, R. E., Jr.; Schwarz, H. A. *Chemical Kinetics*; Prentice Hall: Englewood Cliffs, NJ, 1972.

(2) Levine, R. D.; Bernstein, R. B. *Molecular Reaction Dynamics and Chemical Reactivity*; Oxford University Press: New York, 1987.

(3) Aker, P. M.; Germann, G. J.; Valentini, J. J. *J. Chem. Phys.* **1989**, *90*, 4795−4808.

(4) Lide, D. R. *CRC Handbook of Chemistry and Physics*, 82nd ed.; CRC Press: Boca Raton, FL, 2001.

(5) Schwenke, D. W.; Tucker, S. C.; Steckler, R.; Brown, F. B.; Lynn, G. C.; Truhlar, D. G.; Garret, B. C. *J. Chem. Phys.* **1989**, *90*, 3110.

(6) Parr, C.; Kuppermann, A. Private communication.

(7) Herzberg, G. *Spectra of Diatomic Molecules*, 2nd ed.; Van Nostrand Reinhold: New York, 1950.

(8) Hsiao, M. C.; Sinha, A.; Crim, F. F. *J. Phys. Chem.* **1991**, *95*, 8263−8267.

(9) Sinha, A.; Hsiao, M. C.; Crim, F. F. *J. Chem. Phys.* **1991**, *94*, 4928−4935.

(10) Walch, S. P. *J. Chem. Phys.* **1980**, *72*, 4932−4940.

(11) Schatz, G. C.; Elgersma, H. *Chem. Phys. Lett.* **1980**, *73*, 21−25.

(12) Isaacson, A. D. *J. Chem. Phys.* **1997**, *107*, 3832−3839.

(13) de Aspuru, O.; Clary, D. C. *J. Phys. Chem. A* **1998**, *102*, 9631−9637.

(14) Gerrity, D. P.; Valentini, J. J. *J. Chem. Phys.* **1984**, *81*, 1298−1313.

(15) Marinero, E. E.; Rettner, C. T.; Zare, R. N. *J. Chem. Phys.* **1984**, *80*, 4142−4156.

(16) Germann, G. J.; Huh, Y.-D.; Valentini, J. J. *J. Chem. Phys.* **1992**, *96*, 1957−1966.

(17) Srivastava, A.; Picconatto, C. A.; Valentini, J. J. *J. Chem. Phys.* **2001**, *115*, 2560−2565.

(18) Okabe, H. *Photochemistry of Small Molecules*; John Wiley and Sons: New York, 1978.

(19) Ashfold, M. N. R.; Howe, J. D. *Annu. Rev. Phys. Chem.* **1994**, *45*, 57−82.

(20) Marinero, E. E.; Vasudev, R.; Zare, R. N. *J. Chem. Phys.* **1983**, *78*, 692−699.

(21) Valentini, J. J. Coherent Anti-Stokes Raman Spectroscopy. In *Spectrometric Techniques*; Vanasse, G. A., Ed.; Academic Press: New York, 1985; Vol. 4, pp 1−62.

(22) Truhlar, D. G.; Muckerman, J. T. Reactive Scattering Cross Sections III: Quasiclassical and Semiclassical. In *Atom-Molecule Collision Theory*; Bernstein, R. B., Ed.; Plenum: New York, 1979; pp 505−566.

(23) Aker, P. M.; Valentini, J. J. *Isr. J. Chem.* **1990**, *30*, 157−178.

(24) Simpson, W. R.; Rakitzis, T. P.; Kandel, S. A.; Lev-On, T.; Zare, R. N. *J. Phys. Chem.* **1996**, *100*, 7938−7947.

(25) Picconatto, C. A.; Srivastava, A.; Valentini, J. J. *J. Chem. Phys.* **2001**, *114*, 1663−1671.

(26) van der Zande, W. J.; Zhang, R.; Zare, R. N.; McKendrick, K. G.; Valentini, J. J. *J. Phys. Chem.* **1991**, *95*, 8205−8207.

(27) Kleinermanns, K.; Wolfrum, J. *Chem. Phys. Lett.* **1984**, *104*, 157−159.

(28) Kleinermanns, K.; Linnebach, E.; Wolfrum, J. *J. Phys. Chem.* **1985**, *89*, 2525−2527.

(29) Jacobs, A.; Wahl, M.; Weller, R.; Wolfrum, J. *Chem. Phys. Lett.* **1989**, *158*, 161−166.

(30) Jacobs, A.; Volpp, H.-R.; Wolfrum, J. *J. Chem. Phys.* **1994**, *100*, 1936−1945.

(31) Buelow, S.; Radhakrishnan, G.; Catanzarite, J.; Wittig, C. *J. Chem. Phys.* **1985**, *83*, 444−445.

(32) Radhakrishnan, G.; Buelow, S.; Wittig, C. *J. Chem. Phys.* **1986**, *84*, 727−738.

(33) Buelow, S.; Radhakrishnan, G.; Wittig, C. *J. Phys. Chem.* **1987**, *91*, 5409−5412.

(34) Rice, J.; Hoffmann, G.; Wittig, C. *J. Chem. Phys.* **1988**, *88*, 2841−2843.

(35) Chen, Y.; Hoffmann, G.; Oh, D.; Wittig, C. *Chem. Phys. Lett.* **1989**, *159*, 426−434.

(36) Hoffmann, G.; Oh, D.; Chen, Y.; Engel, Y. M.; Wittig, C. *Isr. J. Chem.* **1990**, *30*, 115−129.

(37) Schatz, G. C.; Fitzcharles, M. S.; Harding, L. B. *Faraday Discuss. Chem. Soc.* **1987**, *84*, 359−369.

(38) Troya, D.; Banos, I.; Gonzalez, M.; Wu, G.; ter Horst, M. A.; Schatz, G. C. *J. Chem. Phys.* **2000**, *113*, 6253−6263.

(39) ter Horst, M. A.; Schatz, G. C.; Harding, L. B. *J. Chem. Phys.* **1996**, *105*, 558−571.

(40) Hammond, G. S. *J. Am. Chem. Soc.* **1955**, *77*, 334−338.

(41) Regan, P. M.; Ascenzi, D.; Clementi, C.; Ashfold, M. N. R.; Orr-Ewing, A. J. *Chem. Phys. Lett.* **1999**, *315*, 187−193.

(42) Aker, P. M.; Germann, G. J.; Valentini, J. J. *J. Chem. Phys.* **1992**, *96*, 2756−2761.

(43) Picconatto, C. A.; Srivastava, A.; Valentini, J. J. *J. Chem. Phys.* **2001**, *114*, 4837−4845.

(44) Huang, J. Quasiclassical trajectory studies of polyatomic reaction dynamics, Ph.D. Thesis, Columbia University, 1995.

(45) Germann, G. J.; Huh, Y.-D.; Valentini, J. J. *J. Chem. Phys.* **1992**, *96*, 5746−5757.

(46) Picconatto, C. A.; Srivastava, A.; Valentini, J. J. *Chem. Phys. Lett.* **2001**, *340*, 317−321.

(47) Srivastava, A.; Picconatto, C. A.; Valentini, J. J. *Chem. Phys. Lett.* **2002**, *354*, 25−30.

(48) Srivastava, A. State-to-state dynamics of the reaction of atomic hydrogen with cyclic alkanes, Ph.D. Thesis, Columbia University, 2000.